

## FEATURED ARTICLE

# Mitophagy alterations in Alzheimer's disease are associated with granulovacuolar degeneration and early tau pathology

Xu Hou<sup>1</sup> | Jens O. Watzlawik<sup>1</sup> | Casey Cook<sup>1</sup> | Chia-Chen Liu<sup>1</sup> | Silvia S. Kang<sup>1</sup> |  
 Wen-Lang Lin<sup>1</sup> | Michael DeTure<sup>1</sup> | Michael G. Heckman<sup>2</sup> | Nancy N. Diehl<sup>2</sup> |  
 Fadi S. Hanna Al-Shaikh<sup>1</sup> | Ronald L. Walton<sup>1</sup> | Owen A. Ross<sup>1,3</sup> |  
 Heather L. Melrose<sup>1</sup> | Nilüfer Ertekin-Taner<sup>1,3,4</sup> | Guojun Bu<sup>1,3</sup> | Leonard Petrucelli<sup>1,3</sup> |  
 John D. Fryer<sup>1,3</sup> | Melissa E. Murray<sup>1,3</sup> | Dennis W. Dickson<sup>1,3</sup> | Fabienne C. Fiesel<sup>1</sup> |  
 Wolfdieter Springer<sup>1,3</sup>

<sup>1</sup> Department of Neuroscience, Mayo Clinic, Jacksonville, Florida, USA

<sup>2</sup> Division of Biomedical Statistics and Informatics, Mayo Clinic, Jacksonville, Florida, USA

<sup>3</sup> Neuroscience PhD Program, Mayo Clinic Graduate School of Biomedical Sciences, Jacksonville, Florida, USA

<sup>4</sup> Department of Neurology, Mayo Clinic, Jacksonville, Florida, USA

**Correspondence**

Wolfdieter Springer or Fabienne C. Fiesel, Department of Neuroscience, Mayo Clinic, 4500 San Pablo Road, Jacksonville, FL 32224, USA.

Email: [Springer.Wolfdieter@mayo.edu](mailto:Springer.Wolfdieter@mayo.edu) (W.S.) or [Fiesel.Fabienne@mayo.edu](mailto:Fiesel.Fabienne@mayo.edu) (F.C.F.)

**Abstract**

**Introduction:** The cytoprotective PTEN-induced kinase 1 (PINK1)-parkin RBR E3 ubiquitin protein ligase (PRKN) pathway selectively labels damaged mitochondria with phosphorylated ubiquitin (pS65-Ub) for their autophagic removal (mitophagy). Because dysfunctions of mitochondria and degradation pathways are early features of Alzheimer's disease (AD), mitophagy impairments may contribute to the pathogenesis.

**Methods:** Morphology, levels, and distribution of the mitophagy tag pS65-Ub were evaluated by biochemical analyses combined with tissue and single cell imaging in AD autopsy brain and in transgenic mouse models.

**Results:** Analyses revealed significant increases of pS65-Ub levels in AD brain, which strongly correlated with granulovacuolar degeneration (GVD) and early phospho-tau deposits, but were independent of amyloid beta pathology. Single cell analyses revealed predominant co-localization of pS65-Ub with mitochondria, GVD bodies, and/or lysosomes depending on the brain region analyzed.

**Discussion:** Our study highlights mitophagy alterations in AD that are associated with early tau pathology, and suggests that distinct mitochondrial, autophagic, and/or lysosomal failure may contribute to the selective vulnerability in disease.

**KEYWORDS**

Alzheimer's disease, autophagy, granulovacuolar degeneration, lysosomes, mitochondria, mitophagy, Parkin, PINK1, PRKN, tau, ubiquitin

## 1 | INTRODUCTION

Alzheimer's disease (AD) is characterized by two main neuropathological hallmarks—amyloid beta (A $\beta$ ) plaques and tau neurofibrillary

tangles. Although the pathogenic mechanisms of AD remain unclear, several studies revealed mitochondrial deficits at very early disease stages<sup>1</sup> and also in preclinical models.<sup>2,3</sup> The mitochondrial cascade hypothesis proposes that the initial decline in mitochondrial

This is an open access article under the terms of the [Creative Commons Attribution-NonCommercial](https://creativecommons.org/licenses/by-nc/4.0/) License, which permits use, distribution and reproduction in any medium, provided the original work is properly cited and is not used for commercial purposes.

© 2020 The Authors. *Alzheimer's & Dementia* published by Wiley Periodicals LLC on behalf of Alzheimer's Association.

function triggers synaptic loss and changes in tau and A $\beta$  homeostasis.<sup>4</sup> In addition, growing evidence also implicates autophagic and lysosomal abnormalities in the pathogenesis of AD.<sup>5-7</sup> This is accompanied and perhaps further aggravated by sustained autophagy induction, which eventually overburdens lysosomal capacities in neurons.<sup>8</sup> Moreover, impaired autophagic flux increases A $\beta$  secretion and plaque formation<sup>9,10</sup> as well as levels of fragmented and hyperphosphorylated tau (p-tau).<sup>11,12</sup>

Another well-documented but poorly understood neuropathological feature of AD is granulovacuolar degeneration (GVD). These intraneuronal accumulations of large double membrane-bound vacuoles harboring a central granule<sup>13</sup> are thought to be late-stage autophagic remnants of incomplete degradation.<sup>14</sup> Although frequently found in normal aging, GVD bodies (GVBs) in patients with AD well exceed age-matched controls.<sup>15</sup> Most prominently located in hippocampal pyramidal neurons, GVBs are also present in other brain regions and in various neurodegenerative disorders.<sup>16,17</sup> In the AD hippocampus, GVD pathology is dependent on pathological tau and its load increases with disease severity.<sup>16</sup> Although the formation of GVBs has been linked to chronic stress conditions,<sup>18-20</sup> their exact origin, nature, and composition are still unknown.

Mitophagy constitutes a key cellular pathway in mitochondrial quality control. Upon stress, the ubiquitin (Ub) kinase PINK1 together with the Ub ligase Parkin/PRKN selectively label terminally damaged mitochondria with phosphorylated serine 65 Ub (pS65-Ub).<sup>21</sup> This specific degradation mark leads to their elimination via the autophagic-lysosomal pathway and thereby preserves the mitochondrial network integrity. Of note, increased mitochondrial dysfunction or impaired autophagic-lysosomal flux lead to the detectable accumulation of the otherwise transient "mitophagy tag" pS65-Ub.<sup>22-24</sup>

Given that all three systems (mitochondria, autophagy, and lysosomes) involved in mitophagy are compromised to some extent in AD, failure of this pathway may play a key role in the disease. Indeed, recent studies have implicated disturbed mitophagy and abnormal PINK1-PRKN signaling in AD pathogenesis, and more importantly have highlighted the therapeutic potential of restoring proper mitophagic flux.<sup>25-28</sup> However, the molecular underpinnings and contribution of different organelles to mitophagy impairments in AD remain unclear. To assess mitophagy alterations in the context of different AD pathologies, we comprehensively measured pS65-Ub levels and distributions in a large series of post-mortem human brains at different disease stages and in two transgenic (Tg) mouse models.<sup>29,30</sup> To better determine the relationship between mitophagy and AD pathologies, we assessed pS65-Ub at both the tissue and single cell level, with a specific focus on the morphology of pS65-Ub-positive structures and their co-localization with different organelles involved in the mitophagy process. Our study further underscores significant mitophagy alterations in AD that may result from distinct organellar impairments and may contribute to the selective vulnerabilities observed in AD and related neurodegenerative disorders.

## RESEARCH IN CONTEXT

1. Systematic review: It is well known that mitochondria, autophagy, and lysosomes are all compromised early in Alzheimer's disease (AD). Furthermore, recent studies have implicated disturbed mitophagy and abnormal PINK1-PRKN signaling in pathogenesis and highlighted the therapeutic potential of targeting this pathway. However, the molecular underpinnings and organellar basis remain unclear.
2. Interpretation: Our study highlights significant mitophagy alterations in AD that track with early tau lesions in human post-mortem brain and transgenic mice. Moreover, our data indicate that mitophagy and granulovacuolar degeneration (GVD) are closely associated and show brain-region-specific alterations that could contribute to selective vulnerabilities observed in disease.
3. Future directions: Autopsy brain from primary tauopathies with different tau isoforms should be analyzed now to characterize the impact of individual species on mitophagy and GVD. Going forward, cultured neurons and animal models will be important to truly understand the dynamics in physiology and pathology and help guide the development of future therapeutics.

## 2 | MATERIALS AND METHODS

### 2.1 | Study subjects

A total of 100 autopsy brains from non-Hispanic Caucasians were retrieved from the Mayo Clinic Florida Brain Bank for biochemical or immunohistochemical analyses (Tables S1 and S2). All brains were examined in a systematic and standardized manner by a single neuropathologist. Available neuropathological information included age at death, Braak stage (0-VI), and Thal phase (0-5), as well as densities of tau tangles and A $\beta$  plaques in hippocampal subregions.<sup>31</sup> Although some specimens had additional comorbid aging-related tau astroglial pathology (ARTAG) and/or TDP-43 pathology, all cases were devoid of Lewy body (LB) pathology (Table S3). In addition to neurologically normal controls, cases with low Braak stage ( $\leq$ III) but high Thal phase ( $>$ 3), and no history of cognitive decline were selected as the pathological aging (PA) cohort<sup>32</sup> to determine the effects of A $\beta$  pathology alone. High Thal phase AD cases with Braak stages IV and V-VI were defined as early-stage AD (esAD) or late-stage AD (lsAD) cohorts, respectively. All AD samples were negative for mutations in known familial early-onset AD genes.

## 2.2 | Immunohistochemistry, immunofluorescence, and image analysis

Immunohistochemical and immunofluorescence staining of paraffin-embedded post-mortem brain tissue was performed as described previously described.<sup>22,24</sup> The used tissue blocks were collected and prepared in a very uniform way, ensuring consistent and comparable representation of regions in all samples. Details for immunostaining and image quantification are described in the supplementary materials.

## 2.3 | Human tissue processing, Meso Scale Discovery enzyme-linked immunosorbent assay (ELISA), and western blot

Frozen human frontal cortex was extracted in 5× volumes of ice-cold radioimmunoprecipitation assay (RIPA) buffer (50 mM Tris, pH 8.0, 150 mM NaCl, 0.1% sodium dodecyl sulfate [SDS], 0.5% deoxycholate, 1% Nonidet P-40, supplemented with protease and phosphatase inhibitors [Sigma-Aldrich, 11697498001 and 04906837001]) to obtain the RIPA-soluble fraction. Post-centrifugation pellets were resuspended in RIPA buffer with 1% SDS and heated at 95°C for 5 minutes to obtain the SDS-soluble fraction. pS65-Ub<sup>51</sup>, tau, p-tau (PHF1), Aβ40, and Aβ42 levels in both fractions were measured using ELISA,<sup>33</sup> and PRKN levels were assessed with western blot.

## 2.4 | Animals, tissue collection, and preparation

Without doxycycline administration, rTg4510 mice used here constitutively express high levels of human P301L tau in the hippocampus and the neocortex.<sup>29</sup> Tissue from sex- and age-matched littermates of 3 and 9 to 11-month-old non-transgenic (nonTg) and rTg4510 Tg mice (n = 3 to 6 per group) were used for immunohistochemistry, subcellular fractionation,<sup>34</sup> western blot, and ELISA. In addition, tissue from sex- and age-matched 9-month-old nonTg (n = 11) and APP/PS1 Tg mice (n = 12)<sup>30</sup> were collected for ELISA.

## 2.5 | Statistical analysis

Non-parametric tests and Spearman tests of correlations were used for human cohorts. For measures in animals, unpaired *t* tests and Pearson test of correlation were used.

Additional details can be found in the supplementary materials and methods section.

## 3 | RESULTS

### 3.1 | pS65-Ub-positive structures are increased in AD autopsy brain

We recently assessed pS65-Ub levels in different brain regions during normal aging and in LB disease and identified significant mitophagy

alterations accompanying the α-synuclein pathology.<sup>24</sup> However, we also observed strong correlations between pS65-Ub and p-tau, although the tau pathology was only minimal and mostly age-related in those cases. Given this striking yet unclear relationship, we expanded our analyses to human AD autopsy brain that was devoid of LB pathology, but presented with a larger range of tau and Aβ pathologies.

We observed two types of pS65-Ub-immunopositive structures in AD brain with differential distribution across individual brain regions (Figure 1A, top): (1) Smaller, solitary structures with punctate appearance that ranged in diameter from 0.6 to 1.7 μm and were particularly prominent in the nucleus basalis of Meynert (nbM); and (2) larger, granular inclusions within vacuoles with a diameter of 3 to 5 μm that were more frequent in the hippocampus and were reminiscent of GVBs. Despite their distinct appearance, both types of granules were positive for the established GVD marker CSNK1D/CK1δ<sup>35</sup> (Figure 1A, bottom). Pre-embedding immunoelectron microscopy confirmed these findings and found individual mitochondria and GVBs heavily labeled with pS65-Ub and occasionally adjacent to pathologic tau filaments (Figure 1B). To further determine the organelle component of pS65-Ub-positive granules, we co-stained hippocampal sections with SSBP1 and CTSD, markers of mitochondria and lysosomes, respectively. Triple staining and 3D image reconstruction revealed a spherical assembly of pS65-Ub-positive vacuolar granules with the mitophagy tag occupying the outer surface that wrapped around both lysosomal structures and mitochondrial components (Figure 1C-F).

To assess pS65-Ub levels in AD autopsy brain by biochemical methods, we first examined lysates from the frontal cortex of neurologically normal controls and AD patients (n = 10 each, Table S1) by Meso Scale Discovery (MSD) ELISA.<sup>51</sup> Compared to controls, AD cases showed significantly increased pS65-Ub levels in both RIPA- (*P* = .0021) and SDS-soluble (*P* = .0089) fractions (Figure 2A). Both fractions also contained higher levels of total tau (RIPA *P* = .0003, SDS *P* = .0001) and p-tau (PHF1) (both fractions *P* < .0001) as well as Aβ40 (RIPA *P* = .0041, SDS *P* = .0004) and Aβ42 (both fractions *P* < .0001) (Figure 2A). pS65-Ub levels correlated significantly with the combined tau or Aβ signals from both fractions, and this correlation was strongest between pS65-Ub and PHF1 (Figure 2B). Given that tau and Aβ measures were strongly correlated, we included additional controls and performed more detailed analysis in later experiments to determine their individual effects. Of note, probing western blots for the Ub ligase PRKN revealed a reduction in RIPA fractions with a concomitant increase in SDS fractions from AD cases, but not controls (Figure 2C). This solubility shift was significant (*P* = .029) and consistent with a previous publication.<sup>28</sup>

### 3.2 | pS65-Ub increases parallel to disease progression in AD and is strongly associated with early tau pathology

To characterize mitophagy alterations in AD on the tissue level, we quantified pS65-Ub-positive cells per area (cell density) in the hippocampus, amygdala, nbM, and putamen by immunohistochemistry.

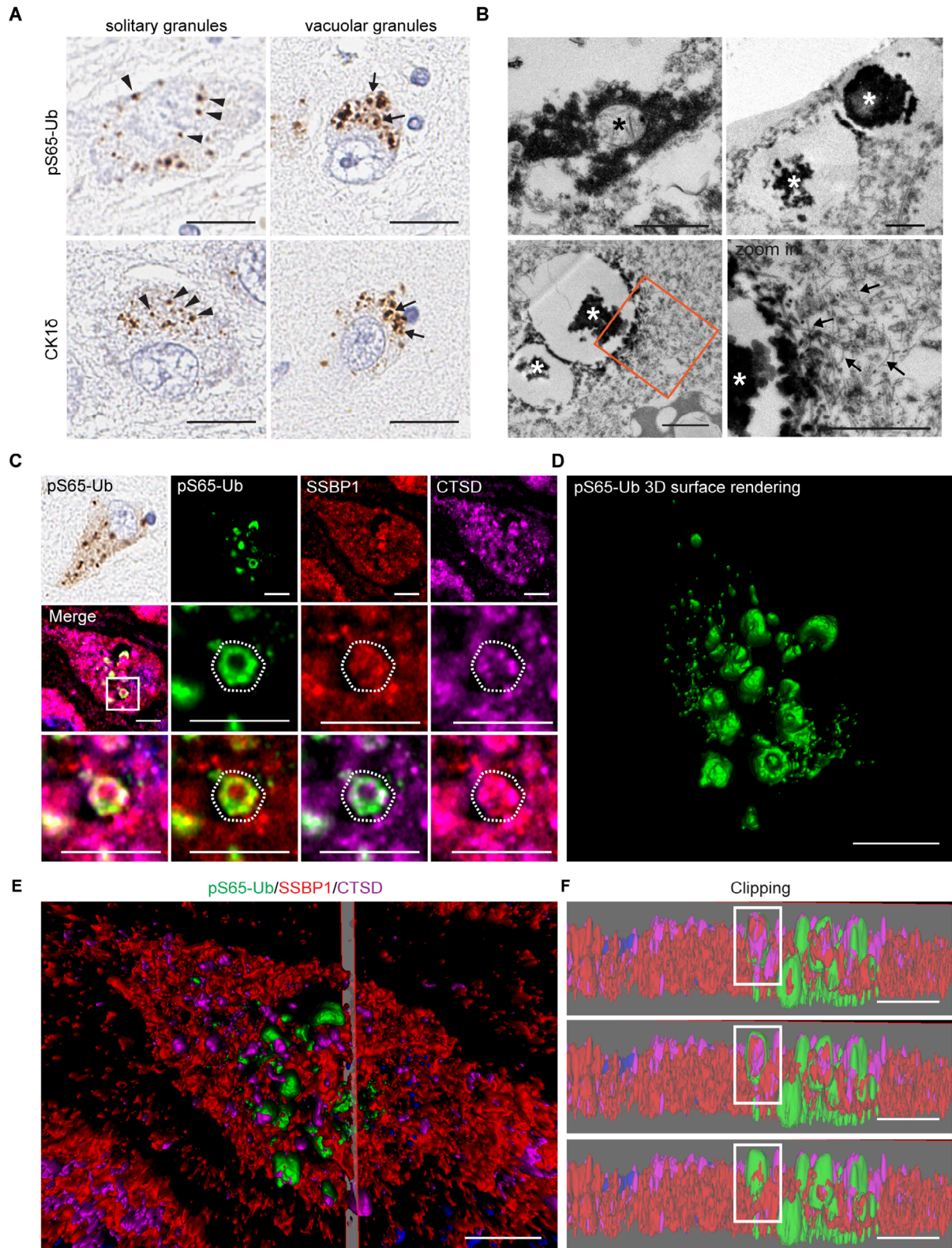


**FIGURE 1** Distinct serine 65 phosphorylated ubiquitin (pS65-Ub) immuno-reactive structures in Alzheimer's disease brain. **(A)** Representative images of pS65-Ub (top) or CK1δ (bottom) immuno-positive solitary (arrowheads) and vacuolar granules (arrows) are shown. Images were taken of neurons from the nucleus basalis of Meynert (left) and hippocampus (right) and show the predominance of the two granular structures in these regions. Scale bars: 20 μm. **(B)** Pre-embedding immunoelectron microscopy shows a mitochondrion (black asterisk) intensely labeled with pS65-Ub (black signal) on the outer membrane (top left). Granulovacuolar degeneration body-like structures (white asterisks) are also labeled with pS65-Ub (top right) and some are adjacent to pathologic tau filaments (bottom, black arrows). The bottom right panel represents the zoom-in view of the selected region (orange square) in the bottom left panel. Scale bars: 1 μm. **(C)** Representative images of two different cells with either

The hippocampus is usually affected first in AD, whereas the amygdala and nbM are affected later and the putamen is often spared. To dissect the individual effects of tau and A $\beta$ , we examined four distinct cohorts ( $n = 20$  each) with varying levels of these AD pathologies (Tables S2-S3). These included age- and sex-matched neurologically normal controls with only minimal tau and A $\beta$  pathology, esAD cases with moderate tau and A $\beta$  pathology and IsAD cases with high tau and A $\beta$  pathology as indicated by their Braak stage and Thal phase (Fig. S1). It is notable that we also analyzed a PA cohort with minimal tau pathology (comparable to controls) and moderate A $\beta$  pathology (comparable to esAD) that allowed us to better discriminate the individual effects of these two AD hallmarks.

Overall, there was a clear brain region-specific increase of pS65-Ub immunoreactivity in both AD cohorts, but not in PA cases (Figure 3A and Figure S2). Similar to GVB lesions (CK1 $\delta$ -positive cell density) and p-tau pathology (CP13-positive cell density), pS65-Ub-positive cell density was highest in the hippocampus, less in the amygdala and nbM, and the least in the putamen. Within individual brain regions, pS65-Ub and CK1 $\delta$  levels were significantly increased in esAD and IsAD but not in PA, in hippocampus and amygdala (both  $P < .0001$ ). Little or no signal was observed in putamen, whereas in the nbM, levels of pS65-Ub but not CK1 $\delta$  were increased in esAD ( $P < .0001$ ) and IsAD (trending toward significance,  $P = .011$ ). Consistent with the cohort selection, there was a gradual increase of tau pathology across the groups from minimal to moderate p-tau levels in controls and PA cases (amygdala  $P = .003$  and nbM  $P = .0062$ ), to moderate and high levels in esAD and IsAD (all regions  $P < .0001$ ).

To characterize the inter-relationship between mitophagy changes and different AD pathologies, we determined associations between pS65-Ub, CK1 $\delta$ , and CP13 levels as well as Braak stage and Thal phase. We found strong correlations between all pairs of measures in the hippocampus, amygdala, and nbM, with the strongest association observed between pS65-Ub and both CK1 $\delta$  and CP13 based on Spearman's  $r$  values (Figure 3B and Figure S3). However, tau and A $\beta$  measures are known to be highly correlated in AD. To dissect individual effects of these two variables, we further used multivariable linear regression models, where a forward selection method was applied after adjusting for age at death and sex as well as for the comorbid ARTAG and TDP-43 pathology (Table S4). Of note, strong and independent associations with pS65-Ub remained in these models only for CK1 $\delta$  and the early p-tau marker CP13, but not for Braak stage that is evaluated based on mature tau tangles or more importantly not for Thal phase that is determined by the presence of A $\beta$  plaques.

To detail individual associations of pS65-Ub with CK1 $\delta$  and particularly early stage tau pathology (CP13), we analyzed hippocampal subregions (Figures S4 and S5A). Compared to controls and PA, pS65-Ub and CK1 $\delta$ -positive cell density was again highest in the earlier affected subregions (subiculum and/or CA1) and significantly higher in both AD

groups, and less in the later affected subregions (CA2/3 and CA4), and only remained significant in the IsAD cohort in CA4. Changes of these two markers were parallel to the gradual progression of tau pathology in the four cohorts, where CP13-positive cell density was increased in both AD groups, whereas mature tau tangle density was increased only in IsAD cases across all subregions (Figure S6). In contrast, A $\beta$  plaque density in PA, esAD, and IsAD groups was elevated to a similar extent compared to controls (Figure S6), consistent with the study design. Although all measures were strongly associated with each other in hippocampal subregions based on Spearman's  $r$  values (Figures S5B and S7), multivariable linear regression analysis with forward selection again revealed independent correlations of pS65-Ub only with CK1 $\delta$  and CP13 levels, and not with tau tangle or A $\beta$  plaque density (Table S5). This further corroborated a strong correlation between mitophagy changes, GVD pathology, and particularly early, but not late-stage tau pathology, and importantly this was independent of A $\beta$  pathology.

### 3.3 | Region-dependent mitophagy changes at the single cell level in AD brain

To further study the relationship between mitophagy changes and early tau pathology, we next co-stained pS65-Ub and p-tau in hippocampal sections where individual neurons showed varying degrees of tau pathology. We categorized pS65-Ub-positive cells based on their p-tau (CP13 and PHF1) status: no p-tau, minor p-tau, and pre-tangle tau aggregation (Figure 4A and Figure S8). Although the percentage of pS65-Ub-positive cells increased already with minor p-tau immunoreactivity (CP13  $P = .038$ , PHF1  $P = .0064$ ), approximately half of pS65-Ub-positive cells contained more advanced tau pathology (pre-tangle stage) (CP13  $P = .0014$ , PHF1  $P = .0059$ ) (Figure 4B). At this stage, pS65-Ub-positive structures appeared to reside within the tau pre-tangle network and this seemed to be accompanied by a more vacuolar appearance (Figure 4C). As expected, no co-existence of pS65-Ub-positive cellular structures and extracellular A $\beta$  plaques was observed in the AD hippocampus (Figure S9). However, GVD pathology has also been described as increasing during development and maturation of tau pathology.<sup>13</sup> To study the relationship between pS65-Ub-positive structures and GVD pathology in single cells, we next co-stained the mitophagy tag and CK1 $\delta$  in different regions, where pS65-Ub- and CK1 $\delta$ -positive structures revealed varying degrees of co-localization (Figure 4D). Of all pS65-Ub-positive cells in the hippocampus and amygdala, over 70% and 50%, respectively, contained primarily vacuolar granules. However,  $\approx 90\%$  of pS65-Ub-positive cells in the nbM contained mainly smaller solitary granules (hippocampus vs nbM  $P < .0001$ , amygdala vs nbM  $P = .0004$ ) (Figure 4E).

A more detailed three-dimensional (3D) analysis of intracellular puncta with double immunofluorescence staining (Figure 4F, top)

---

immunohistochemical staining (top left corner) or immunofluorescence staining (the rest images). pS65-Ub-positive structures (green) and lysosomes (CTSD, purple) seem to form elongated spheres that closely decorate mitochondrial aggregates (SSBP1, red). Scale bars: 5  $\mu\text{m}$ . (D) 3D surface reconstruction of pS65-Ub-positive structures and (E, F) three consecutive planes of 3D clipping of one triple-labeled granule (white rectangles) are shown. Scale bars: 5  $\mu\text{m}$

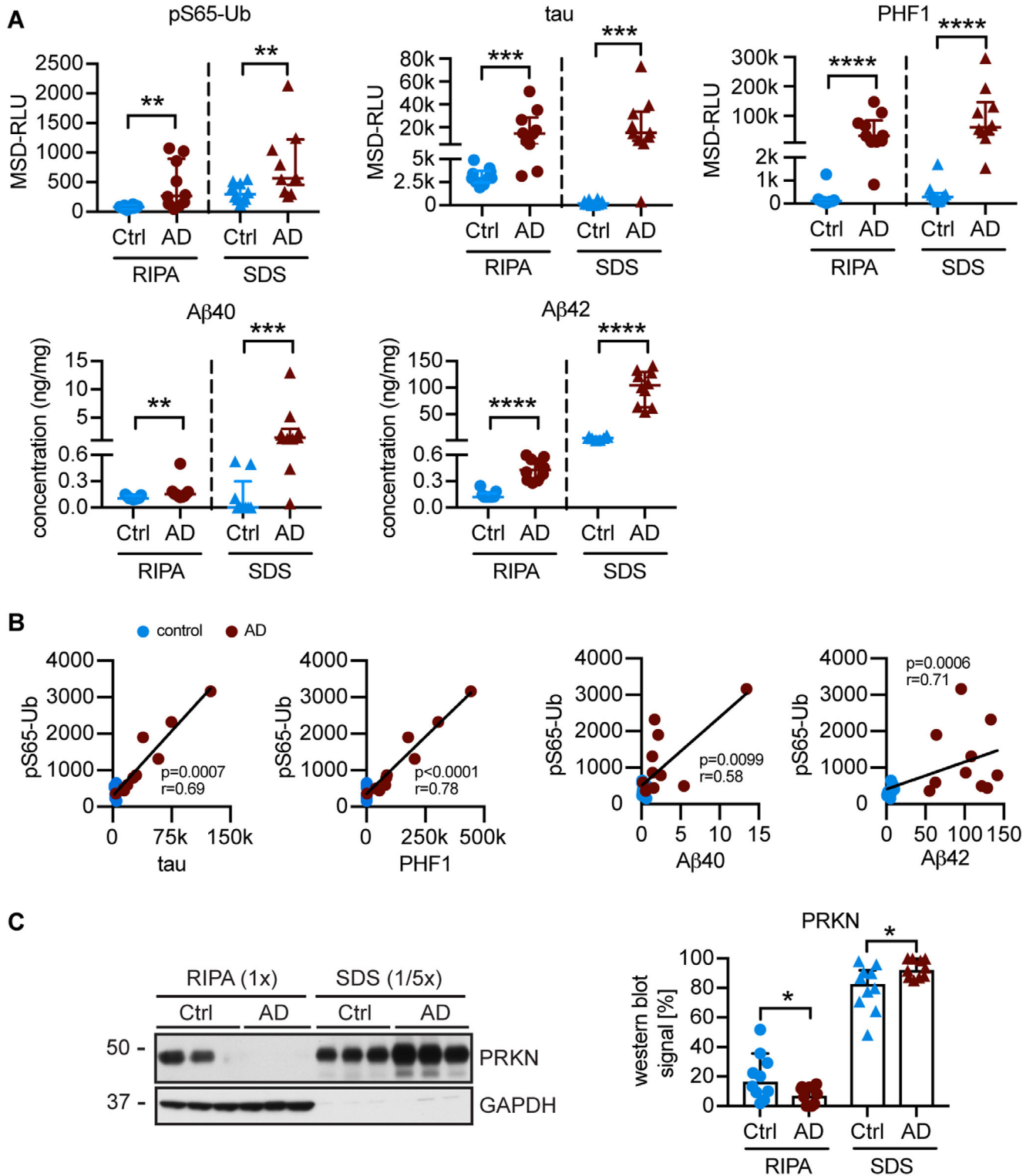


**FIGURE 2** Levels of mitophagy-related markers and Alzheimer's disease (AD) pathology markers in human brain lysate. (A) Meso Scale Discovery enzyme-linked immunosorbent assay (ELISA) show increased levels of phosphorylated serine 65 ubiquitin (pS65-Ub), total tau, PHF1, amyloid beta ( $A\beta$ ) 40, and  $A\beta$ 42 in both radioimmunoprecipitation assay (RIPA) buffer and sodium dodecyl sulfate (SDS)-soluble fractions of brain lysates from AD frontal cortex compared to controls (Mann-Whitney  $U$  test followed by adjustment with Bonferroni correction,  $*P < .025$  [ie, the statistical significance threshold after Bonferroni correction],  $**P < .01$ ,  $***P < .001$ ,  $****P < .0001$ ). (B) pS65-Ub levels are strongly correlated with tau, PHF1,  $A\beta$ 40, and  $A\beta$ 42 levels in combined signals from both fractions (Spearman test of correlation, significance threshold after Bonferroni correction:  $P < .025$ ). (C) Representative western blot of lysates from three controls and three AD cases showing a shift of parkin RBR E3 ubiquitin protein ligase (PRKN) from the RIPA- to the SDS-soluble fraction (left). Western blot quantification of soluble (RIPA fraction) and insoluble (SDS fraction) PRKN as a percentage of total PRKN protein in control and AD brain lysates (right) (Mann-Whitney  $U$  test,  $*P < .05$ ).  $n = 10$  per group. Data shown as median with interquartile range

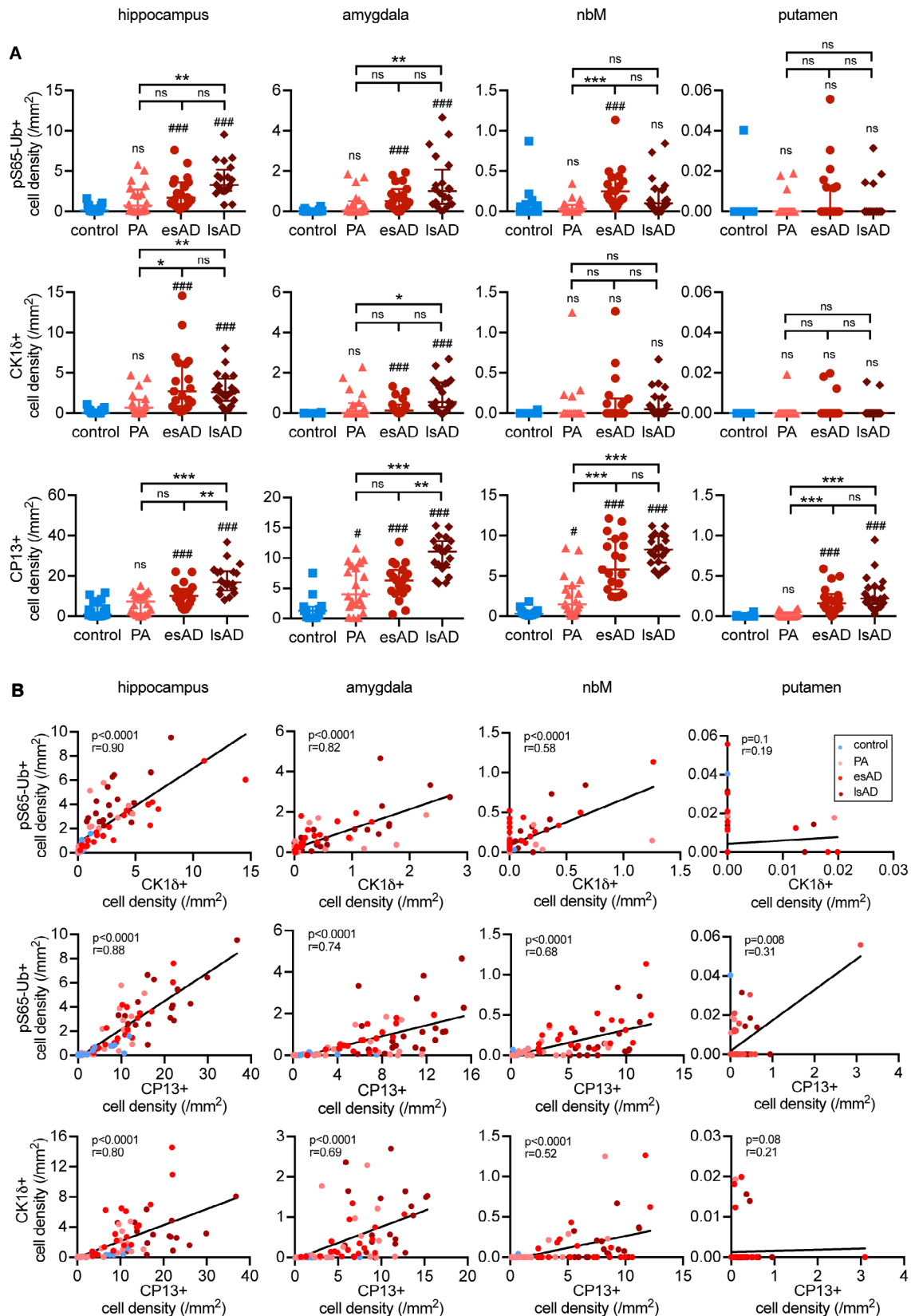


**FIGURE 3** Quantification and correlations of phosphorylated serine 65 ubiquitin (pS65-Ub)-, CK1δ-, and CP13-positive cells in autopsy brain. (A) Levels of pS65-Ub-, CP13-, and CK1δ-positive cell density are increased differentially in the hippocampus, amygdala, nucleus basal of Meynert (nbM), and putamen in early-stage Alzheimer's disease (esAD) and late-stage Alzheimer's disease (lsAD) cohorts. Number signs (#) on top of the groups show the significance levels compared to controls, while asterisks (\*) show the significance level between two disease groups as indicated by brackets (Kruskal-Wallis and Mann-Whitney *U* tests followed by adjustment with Bonferroni correction, # or \* *P* < .0083 [ie, the statistical significance threshold after Bonferroni correction], ## or \*\* *P* < .001, ### or \*\*\* *P* < .0001, ns - not significant). Data shown as median with interquartile range. (B) pS65-Ub-, CP13-, and CK1δ-positive cell density are strongly correlated with each other in all four brain regions with the strongest correlation in the hippocampus (Spearman test of correlation, significance threshold: *P* < .0125). Controls: *n* = 18 for hippocampus and putamen, *n* = 17 for amygdala, *n* = 19 for nbM; Pathological aging (PA) and lsAD: *n* = 20 each for all regions; esAD: *n* = 19 for all regions

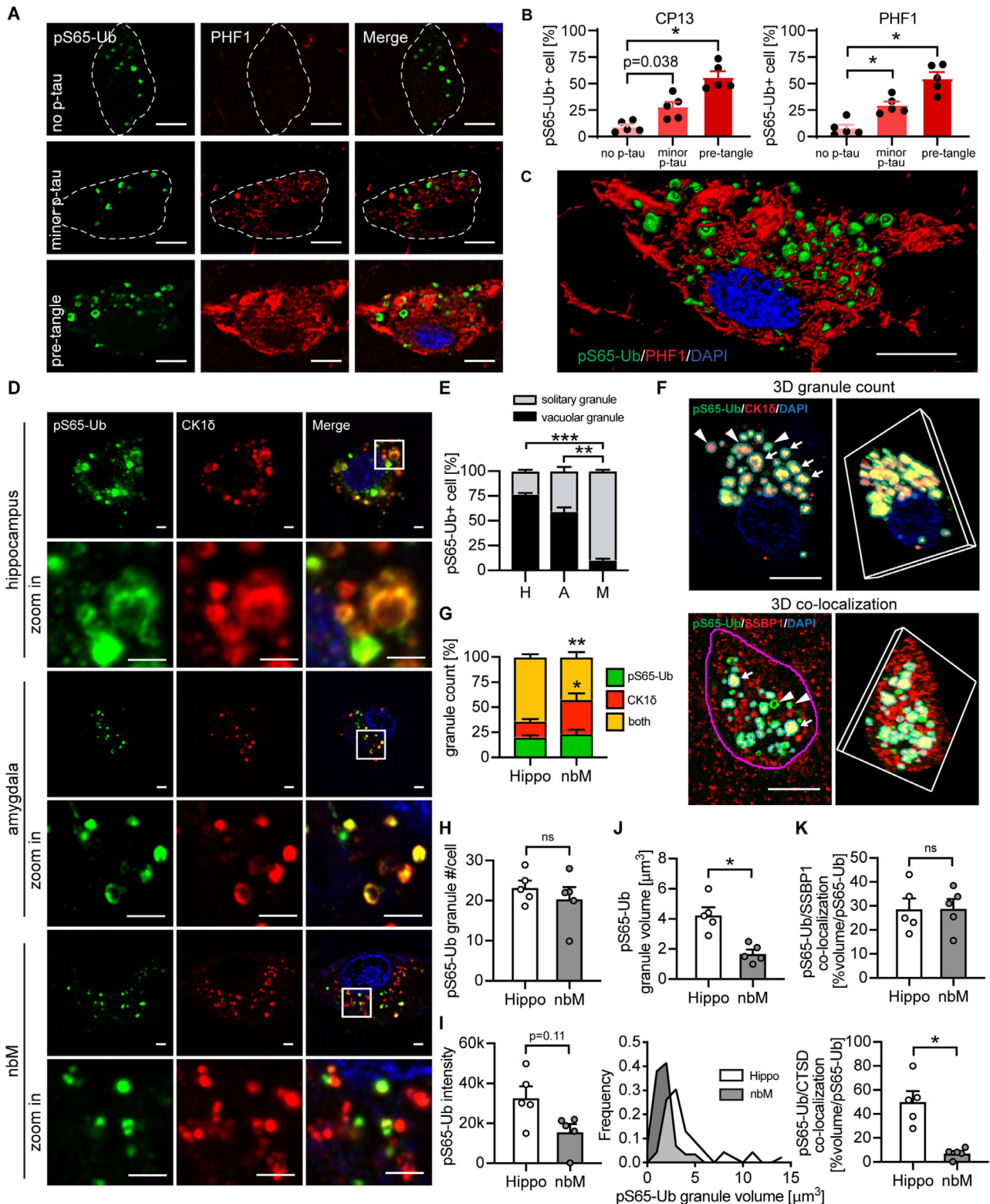


**FIGURE 4** Relationship of phosphorylated serine 65 ubiquitin (pS65-Ub)-positive structures with early tau pathology, granulovacuolar degeneration pathology, and cell organelle markers in Alzheimer's disease (AD) brain. **(A)** Representative images from the hippocampus showing pS65-Ub-positive cells (green) with different stages of hyperphosphorylated tau (p-tau) pathology (PHF1, red): no p-tau, minor p-tau, and pre-tangle tau aggregation. Dashed lines were used to contour the cells. Scale bar: 5  $\mu\text{m}$ . **(B)** The percentage of hippocampal pS65-Ub-positive cells in different stages of p-tau pathology (no p-tau, minor p-tau, or pre-tangle tau aggregation) as determined by CP13 or PHF1 staining is shown. (paired *t* test, \**P* < .0083 [ie the statistical significance threshold after Bonferroni correction]). *n* = 5. **(C)** 3D surface reconstruction of a cell co-stained with pS65-Ub (green) and PHF1 (red) at pre-tangle tau aggregation stage. Scale bars: 5  $\mu\text{m}$  **(D)** Human brain sections from AD cases are double labeled with antibodies against pS65-Ub and CK1 $\delta$ . Representative images from the hippocampus, amygdala, and nucleus basalis of

revealed that hippocampal neurons contained mostly pS65-Ub- and CK1 $\delta$ -double-positive granules, which was significantly higher than in nbM neurons ( $P = .0056$ ). However, nbM neurons had a higher percentage of CK1 $\delta$ -only-positive granules ( $P = .033$ ) compared to hippocampal neurons (Figure 4G). Yet the absolute number of pS65-Ub-positive granules (pS65-Ub only plus pS65-Ub-CK1 $\delta$  co-stained) per cell was similar in these two regions (Figure 4H). Although the hippocampal granules appeared brighter, there was no statistically significant difference in signal intensity (Figure 4I), but these granules were significantly larger than the ones in the nbM ( $P = .012$ ), consistent with their predominant vacuolar, as opposed to solitary appearance in the hippocampus (Figure 4J).

Given the diverse morphology and co-localization profiles of pS65-Ub-positive structures in the hippocampus and nbM, we next determined their organelle components by co-staining of pS65-Ub with SSBP1 or CTSD (Figure S10) followed by 3D co-localization analysis (Figure 4F, bottom). Similar to the pS65-Ub-positive structures, both mitochondria and lysosomes appeared condensed and formed intensely labeled, large granules in the hippocampus. In contrast, both organelles were more scattered throughout the cells and were relatively weakly labeled in nbM neurons. Co-localization of pS65-Ub with mitochondria was similar in both regions (Figure 4K), whereas its co-localization with lysosomes was significantly higher in the hippocampus compared to nbM ( $P = .011$ ). Together, these findings underscore tau pathology-dependent and brain region-specific alterations of mitophagy in AD. The diverse co-localization profiles of pS65-Ub-positive granules in individual neurons from different brain regions further highlight that distinct mitochondrial or lysosomal impairments may contribute to the selective vulnerability in neurodegenerative diseases.<sup>36</sup>

### 3.4 | Increases of pS65-Ub in rTg4510 mice are associated with early tau pathology

Given that fixed tissue from end-stage human disease does not allow an assessment of the mitophagy pathway during the progression of the pathology, we validated our findings in rTg4510 mice that accumulate argyrophilic tangle-like inclusions in the cortex by 4 months of age and in the hippocampus after 5.5 months.<sup>29</sup> Although pS65-Ub and CK1 $\delta$  signals were undetectable by immunostaining in brains of

3-month-old animals, immunoreactivity of pS65-Ub was strongly increased in 9 to 11-month-old Tg mice compared to age-matched nonTg littermates (hippocampus  $P = .003$ , cortex  $P = .0027$ ) (Figure 5A-C). CK1 $\delta$ -positive cell density was significantly increased too in both brain regions at 9 to 11-month of age (hippocampus  $P = .0027$ , cortex  $P = .0088$ ). Multi-color immunofluorescence showed that pS65-Ub signals were mainly present in cells with tau inclusions and partially co-localized with CP13, PHF1, and CK1 $\delta$  in tau Tg brains (Figure 5D), similar to in human AD brain.

MSD ELISA measurements confirmed the increased levels of pS65-Ub ( $P = .002$ ), tau ( $P = .0004$ ), and PHF1 ( $P = .0001$ ) in total brain lysates from 11-month-old Tg mice. It is notable that in contrast to immunohistochemistry, this highly sensitive pS65-Ub MSD assay<sup>51</sup> allowed us to detect increased levels of the mitophagy tag ( $P = .0016$ ) already in 3-month-old Tg compared to nonTg animals. At this age, mice showed an increase of total tau ( $P < .0001$ ), but this was prior to the significant accumulation of p-tau pathology (Figure 6A,B). Consistent with results from human brain, analyses showed significant correlations of pS65-Ub with both total tau and PHF1. In addition to increased levels of tau, PHF1, and PRKN ( $P = .035$ ) in western blots of total brain lysates (Figure 6C), higher amounts of total tau and PHF1 as well as higher molecular weight tau species were detected in mitochondrial and cytosolic fractions in 9-month-old Tg but not in nonTg mice (Figure 6D). This increase was accompanied by an enhanced translocation of PRKN from the cytosol to mitochondria, which is commensurate with the level of mitochondrial damage and the activation of mitophagy.

To further ascertain the dependence on tau, but not A $\beta$ , we measured pS65-Ub levels also in APP/PS1 Tg mice. As expected, MSD ELISA measurements failed to detect any differences in pS65-Ub levels from cortical lysates of 9-month-old nonTg or APP/PS1 animals. However, the Tg mice exhibited significantly higher levels of A $\beta$ 40 and A $\beta$ 42 (both  $P < .0001$ ) as measured by ELISA (Figure 6E). No correlation between pS65-Ub and A $\beta$ 40 or A $\beta$ 42 levels was observed (Figure 6F). Altogether, these results suggest similar tau but not A $\beta$  pathology-dependent mitophagy alterations in Tg animals as seen in human AD brain. This now opens up opportunities to further dissect the contributions of mitochondrial, autophagic, and/or lysosomal dysfunctions in individual brain cells *in vivo* over time during the build-up and progression of tau pathology.

Meynert (nbM) are shown. Greater co-localizations of pS65-Ub- and CK1 $\delta$ -positive granules are found in the hippocampus and amygdala compared to nbM. As indicated, zoom-in images of the white square regions are shown in the respective rows below. Scale bars: 2  $\mu$ m. (E) Percentage of pS65-Ub-positive cells with mainly either solitary or vacuolar granules is shown for different brain regions: H – hippocampus, A – amygdala, M – nbM (paired *t* test, \* $P < .0167$  [ie, the statistical significance threshold after Bonferroni correction], \*\* $P < .001$ , \*\*\* $P < .0001$ )  $n = 5$  for all regions. (F) AD hippocampal and nbM sections are co-stained with pS65-Ub (green) and CK1 $\delta$  (red) or mitochondrial marker (SSBP1, red) or lysosomal marker (CTSD, not shown) for the single cell quantification. Representative images of the 3D single cell quantification for granule count (top) and co-localization (bottom) are shown. Arrows and arrowheads point to granules/area that were immuno-positive for both antibodies or only one antibody, respectively. Scale bars: 5  $\mu$ m. (G) Percentage of granules per cell in the hippocampus and nbM that are co-localized with signals of either pS65-Ub only (green), CK1 $\delta$  only (red), or both (yellow). (H) pS65-Ub-positive granule count per cell. (I) Intensity of the pS65-Ub signal. (J) Average individual granule volume per cell (top) and their distribution (bottom) in the hippocampus and nbM. (K) Percentage of pS65-Ub-positive signals that co-localize with mitochondrial marker (top) or lysosomal marker (bottom) in the hippocampus and nbM. (paired *t* test, \* $P < .05$ , \*\* $P < .01$ , ns – not significant)  $n = 5$  for both regions. Data shown as mean with SEM

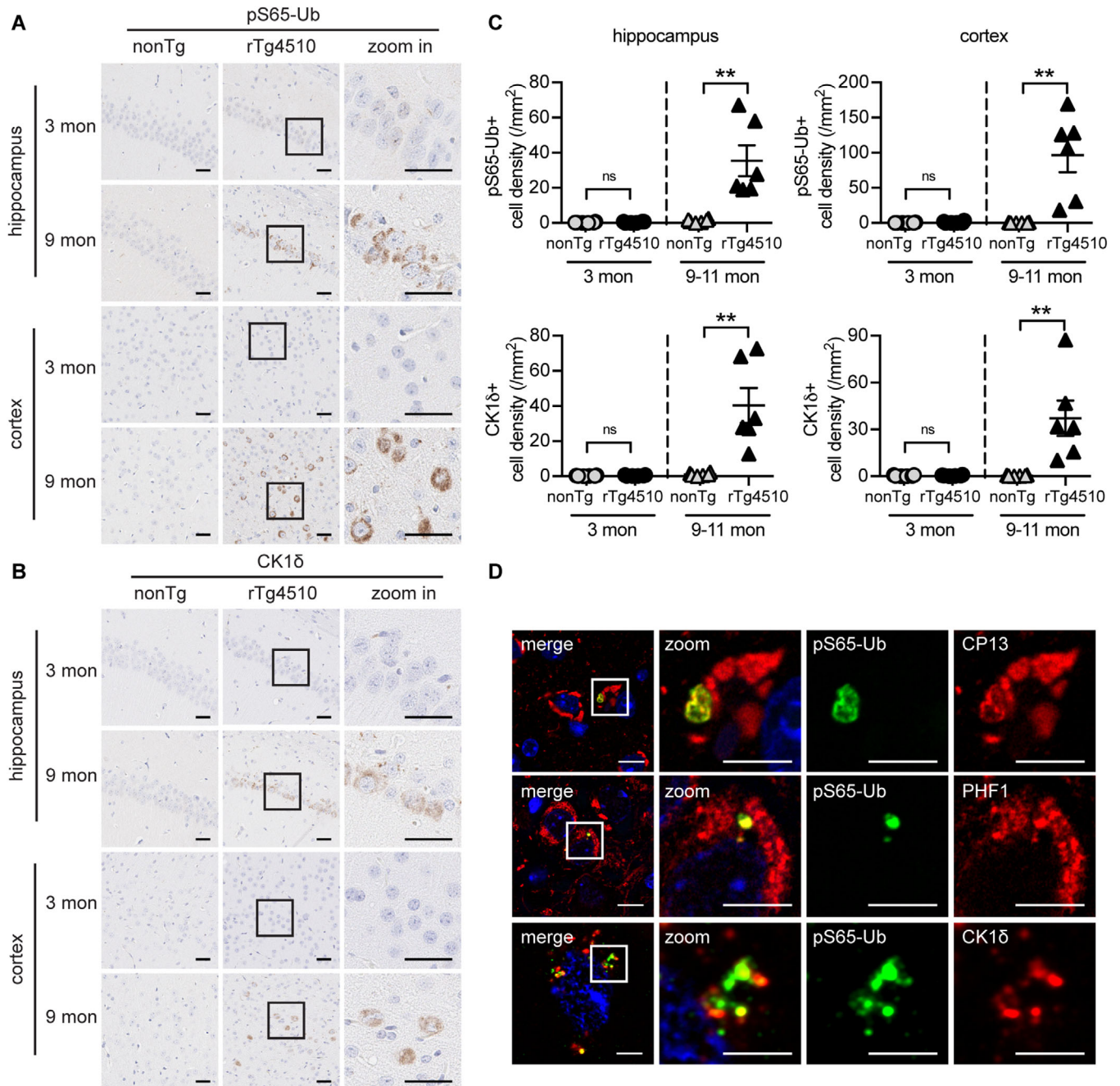


**FIGURE 5** Age-dependent increases of phosphorylated serine 65 ubiquitin (pS65-Ub) and CK1 $\delta$  levels in rTg4510 mouse brains. (A-C) Immunohistochemical analyses of pS65-Ub- and CK1 $\delta$ -positive cells in sections from age- and sex-matched rTg4510 and non-transgenic (nonTg) mice. Nine to 11 month but not 3-month-old rTg4510 mice have increased pS65-Ub- and CK1 $\delta$ -positive cell densities in the hippocampus and cortex compared to age-matched nonTg mice (unpaired *t* test, \**P* < .05, \*\**P* < .01, ns – not significant). *n* = 6 per group. Data shown as mean with SEM. Scale bars: 10  $\mu$ m. (D) pS65-Ub labeled structures co-localize with hyperphosphorylated tau (CP13 and PHF1) and CK1 $\delta$  signals in the hippocampus of 9-month-old rTg4510 mice. Scale bar: 5  $\mu$ m

#### 4 | DISCUSSION

Accumulating evidence suggests that mitochondrial and autophagolysosomal dysfunctions are among the earliest detectable signs and promote the disease-defining pathologies in AD.<sup>37</sup> Impaired mitophagy results in oxidative stress and bioenergetic deficits that

trigger A $\beta$  and tau aggregation, which in turn compromises selective degradation of damaged mitochondria.<sup>26,28,38,39</sup> Loss of PINK1-PRKN aggravates pathologies, synapse loss, and cognitive dysfunction in AD mouse models,<sup>40,41</sup> whereas overexpression of either gene or mitophagy stimulation appears to ameliorate these phenotypes.<sup>25,27,42</sup> Besides a prominent role in the pathogenesis of PD, mitophagy is now

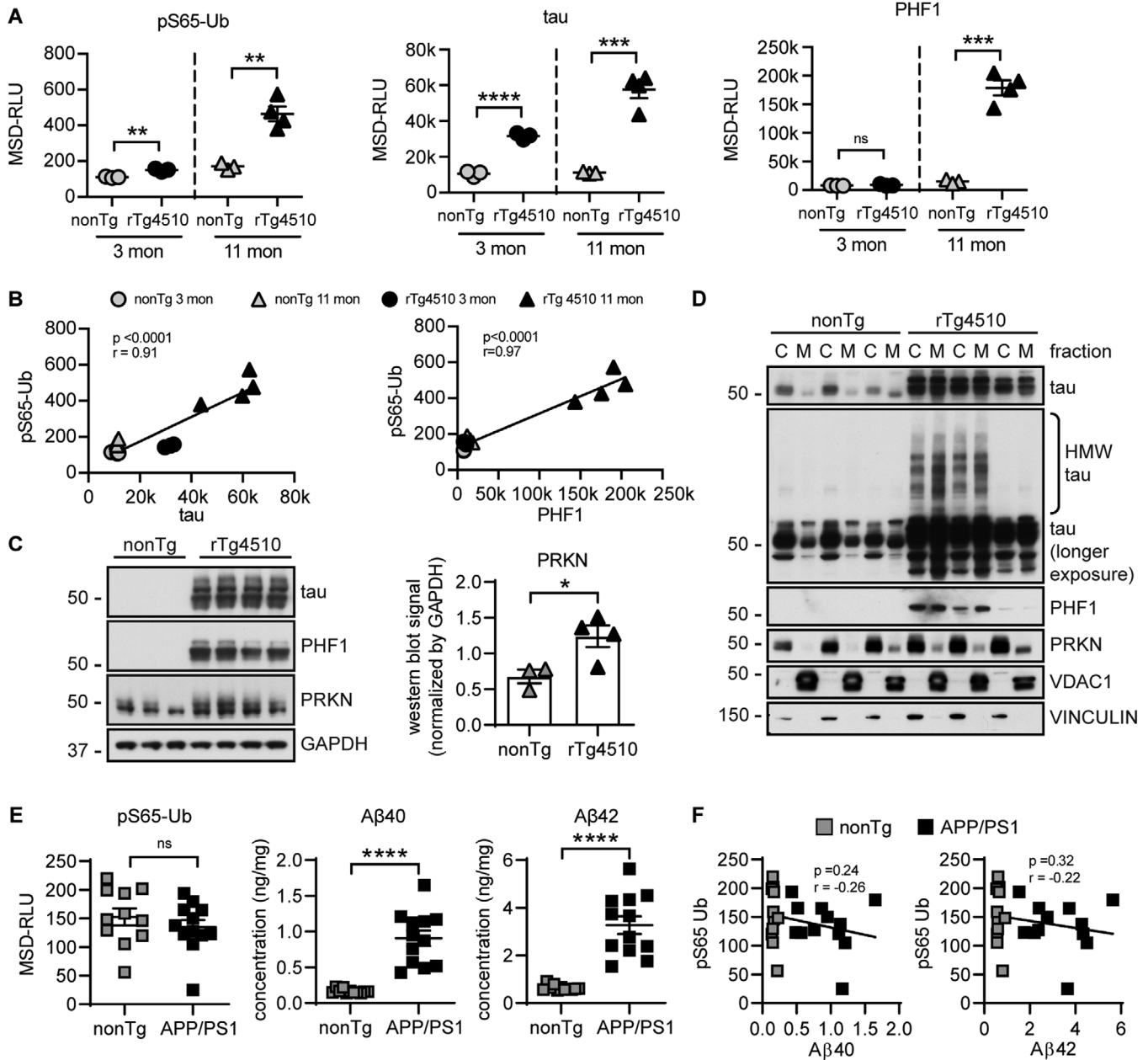


**FIGURE 6** Increases of mitophagy-related proteins in rTg4510 but not in APP/PS1 mouse brains. (A) Meso Scale Discovery (MSD) enzyme-linked immunosorbent assay (ELISA) shows increased phosphorylated serine 65 ubiquitin (pS65-Ub), total tau, and PHF1 levels in total brain lysates of 11-month-old rTg4510 mice compared to age-matched non-transgenic (nonTg) mice. Only the former two measures also increase in 3-month-old rTg4510 mice.  $n = 3$  for nonTg and  $n = 4$  for rTg4510 mice for both age groups (unpaired  $t$  test,  $*P < .05$ ,  $**P < .01$ ,  $***P < .001$ ,  $****P < .0001$ , ns – not significant). (B) pS65-Ub levels are significantly correlated with both total tau (left) and PHF1 (right) levels in total brain lysates. (Pearson test of correlation, significance threshold:  $P < .05$ ). (C) Western blot shows increased total tau, PHF1, and parkin RBR E3 ubiquitin protein ligase (PRKN) levels in total brain lysates of 11-month rTg4510 mice compared to nonTg controls (left). The quantification of PRKN blots shows a significant difference (right).  $n = 3$  for nonTg and  $n = 4$  for rTg4510 mice (unpaired  $t$  test,  $*P < .05$ ). (D) Mitochondrial fractions (M) of mouse brain lysates contain higher levels of total tau, higher molecular weight (HMW) tau, PHF1, and PRKN in 9-month rTg4510 mice than age-matched nonTg mice. Separation into mitochondrial (M) and cytoplasmic (C) fractions was verified using antibodies against VDAC1 and VINCULIN, respectively.  $n = 3$  per group. (E) MSD ELISA shows no differences of pS65-Ub levels in cortical lysates from 9-month-old APP/PS1 mice compared to age- and sex-matched nonTg mice. Both amyloid beta ( $A\beta$ ) 40 and 42 levels are significantly increased in APP/PS1 mice as measured by ELISA. (unpaired  $t$  test,  $*P < .05$ ,  $****P < .0001$ , ns – not significant) (F) No correlation between pS65-Ub and  $A\beta$ 40 or 42 levels is observed in 9-month-old nonTg and APP/PS1 mice. (Pearson test of correlation, significance threshold:  $P < .05$ ).  $n = 11$  for nonTg and  $n = 12$  for APP/PS1 mice. Data shown as mean with SEM

being appreciated as a key modifier and potential neuroprotective avenue also for AD. However, mechanisms and involved organelles, cell type-specific effects, and the order of events during a vicious interplay between mitophagy failure and pathology especially in larger human autopsy brain series remain unclear. Recently, we had observed a strong association of pS65-Ub with minimal, age-related tau pathology in human autopsy brain.

Here, we corroborated our findings using a much larger series of AD samples with varying levels of tau burden, but similar amyloid load, and characterized region-specific correlations between mitophagy alterations and neuropathologies. The significantly increased pS65-Ub levels in AD were especially high in the most vulnerable regions. We also demonstrated strong and independent correlations of pS65-Ub with GVD and early p-tau pathology, but not mature tau tangles or A $\beta$  plaques. Two recent studies reported an interaction between tau, PRKN, and mitophagy, although opposing effects and different mechanisms were suggested that may be attributable to distinct tau species.<sup>26,38</sup> However, evidence *in vivo* and in human autopsy brain has remained scarce. Although pS65-Ub acts as the mitophagy tag, it also serves as an allosteric activator and receptor for PRKN on damaged mitochondria.<sup>21</sup> In brain, pS65-Ub granules appeared to reside in the forming tangles, which could lead to a sequestration of PRKN and thus depletion of this vital Ub ligase away from the soluble compartment. Indeed, in addition to a significant solubility shift of PRKN protein in AD brain,<sup>28</sup> we also observed increased levels of PRKN in the mitochondrial compartment in brains from tau Tg mice. It will now be important to refine the impact and mechanisms of individual tau species and to expand analyses to brains with primary tauopathies that present with different types of tau aggregation.

Although we found strong effects of early tau pathology in both human AD brain and Tg mice, our analyses did not show independent correlations of pS65-Ub A $\beta$  peptides or late-stage, extracellular plaques. However, numerous studies had reported direct effects of intracellular A $\beta$  on mitochondria<sup>37,43</sup> and some even suggested a reciprocal relationship with PINK1-PRKN-dependent mitophagy.<sup>25,27,28,42</sup> Moreover, it is well known that genes that promote  $\beta$ -amyloidogenesis have primary effects on the endosomal-autophagy-lysosomal network<sup>10</sup> and thus also impact mitophagy. In the future it will be critical to assess the involvement of AD genes and risk factors and their effects on different organelles and mechanisms involved in mitophagy.

In addition to a strong morphological similarity between structures labeled by the mitophagy tag pS65-Ub and the GVD marker CK1 $\delta$ , both are formed as part of a stress response<sup>21,44</sup> and increase with aging, but are much more frequent in AD.<sup>15,16,24</sup> Ultrastructurally, GVD bodies present as intraneuronal, double membrane-bound, cytoplasmic vacuoles with autophagic and lysosomal components.<sup>14,44,45</sup> However, not all CK1 $\delta$ -positive granules appeared with the typical double-membrane structures. Rather CK1 $\delta$  and pS65-Ub both labeled smaller solitary as well as larger vacuolar granules, which might reflect distinct organellar impairments in the respective brain regions. In the nbM, pS65-Ub immunoreactivity was found mostly on smaller solitary

granules that were positive for mitochondrial, but not lysosomal markers. In the hippocampus, pS65-Ub-positive granules were larger with a vacuolar appearance reminiscent of typical GVBs. These structures were also positive for both mitochondrial and lysosomal markers. Although our study underscores prominent mitophagy impairments in AD, it further emphasizes that, depending on the brain region, these alterations may arise through enhanced mitochondrial stress, stalled trafficking, or reduced autophagic-lysosomal flux and may contribute to the selective vulnerabilities observed in AD.<sup>46</sup>

To truly understand the dynamics of and cross-talk between these organelles in different neuronal subtypes, live cell analyses should be performed to monitor morphology, function, and health in, for example, induced pluripotent stem cell-derived neurons. These can be combined with *in vivo* readouts from emerging animal models expressing ratiometric reporters to monitor flux of general<sup>47</sup> or selective autophagy<sup>48,49</sup> over time during the progression of pathology. Together, this may lead to a better understanding of organellar and neuronal function in physiological and pathological environments. Of note, induction of mitophagy might be beneficial early in AD, but could be detrimental at more advanced stages due to upregulated autophagy and a progressively declined lysosomal capacity.<sup>8,50</sup> Detailed elucidation of the brain region-dependent organellar dysfunctions at different disease stages will help guide future therapies that may facilitate autophagy induction while ensuring proper flux and effective degradation.

#### ACKNOWLEDGMENTS

We are grateful to the patients and their families who made this study possible. We thank Monica Castanedes-Casey, Linda G. Rousseau, Virginia R. Phillips, Billie J. Matchett, and Sydney A. Labuzan from the Neuropathology Laboratory for processing human post-mortem tissues and the excellent technical support. We also thank Dr. Peter Davies from the Feinstein Institute for his generous contribution of p-tau antibodies.

W.S. is partially supported by the National Institutes of Health National Institute on Aging (NIH/NIA) [R56 AG062556], National Institute of Neurological Disorders and Stroke (NIH/NINDS) [R01/RF1 NS085070 and U54 NS110435], the Department of Defense Congressionally Directed Medical Research Programs (CDMRP) [W81XWH-17-1-0248], the Florida Department of Health - Ed and Ethel Moore Alzheimer's Disease Research Program [9AZ10], the Michael J. Fox Foundation for Parkinson's Research (MJFF), and the Mayo Clinic Foundation and the Center for Biomedical Discovery (CBD). X.H. is supported by a pilot grant from the Mayo Clinic Alzheimer's Disease Research Center (ADRC) and a fellowship awarded by the American Parkinson Disease Association (APDA). F.C.F. is the recipient of fellowships from the Younkin Scholar Program and the APDA and is supported in part by the MJFF and a Gerstner Family Career Development Award from the Mayo Clinic Center for Individualized Medicine (CIM). L.P., C.C., and D.W.D. are supported by the NIH/NINDS [U54 NS100693] and L.P. is supported by NIH/NINDS [R35 NS097273]. G.B. is supported by NIH/NIA [R37 AG027924].

## CONFLICT OF INTEREST

Mayo Clinic, W.S., and F.C.F. have filed a patent in the area of mitophagy activation.

## REFERENCES

- Gibson GE, Shi Q. A mitocentric view of Alzheimer's disease suggests multi-faceted treatments. *J Alzheimers Dis.* 2010;20(suppl 2):S591-S607.
- Fu YJ, Xiong S, Lovell MA, Lynn BC. Quantitative proteomic analysis of mitochondria in aging PS-1 transgenic mice. *Cell Mol Neurobiol.* 2009;29:649-664.
- Hauptmann S, Scherping I, Drose S, et al. Mitochondrial dysfunction: an early event in Alzheimer pathology accumulates with age in AD transgenic mice. *Neurobiol Aging.* 2009;30:1574-1586.
- Swerdlow RH, Burns JM, Khan SM. The Alzheimer's disease mitochondrial cascade hypothesis: progress and perspectives. *Biochim Biophys Acta.* 2014;1842:1219-1231.
- Boland B, Kumar A, Lee S, et al. Autophagy induction and autophagosome clearance in neurons: relationship to autophagic pathology in Alzheimer's disease. *J Neurosci.* 2008;28:6926-6937.
- Lee S, Sato Y, Nixon RA. Lysosomal proteolysis inhibition selectively disrupts axonal transport of degradative organelles and causes an Alzheimer's-like axonal dystrophy. *J Neurosci.* 2011;31:7817-7830.
- Nixon RA, Wegiel J, Kumar A, et al. Extensive involvement of autophagy in Alzheimer disease: an immuno-electron microscopy study. *J Neuropathol Exp Neurol.* 2005;64:113-122.
- Bordi M, Berg MJ, Mohan PS, et al. Autophagy flux in CA1 neurons of Alzheimer hippocampus: increased induction overburdens failing lysosomes to propel neuritic dystrophy. *Autophagy.* 2016;12:2467-2483.
- Nilsson P, Loganathan K, Sekiguchi M, et al. Abeta secretion and plaque formation depend on autophagy. *Cell Rep.* 2013;5:61-69.
- Nixon RA. Amyloid precursor protein and endosomal-lysosomal dysfunction in Alzheimer's disease: inseparable partners in a multifactorial disease. *FASEB J.* 2017;31:2729-2743.
- Wang Y, Martinez-Vicente M, Kruger U, et al. Tau fragmentation, aggregation and clearance: the dual role of lysosomal processing. *Hum Mol Genet.* 2009;18:4153-4170.
- Inoue K, Rispoli J, Kaphzan H, et al. Macroautophagy deficiency mediates age-dependent neurodegeneration through a phospho-tau pathway. *Mol Neurodegener.* 2012;7:48.
- Kohler C. Granulovacuolar degeneration: a neurodegenerative change that accompanies tau pathology. *Acta Neuropathol.* 2016;132:339-359.
- Funk KE, Mrak RE, Kuret J. Granulovacuolar degeneration (GVD) bodies of Alzheimer's disease (AD) resemble late-stage autophagic organelles. *Neuropathol Appl Neurobiol.* 2011;37:295-306.
- Xu M, Shibayama H, Kobayashi H, et al. Granulovacuolar degeneration in the hippocampal cortex of aging and demented patients—a quantitative study. *Acta Neuropathol.* 1992;85:1-9.
- Yamazaki Y, Matsubara T, Takahashi T, et al. Granulovacuolar degenerations appear in relation to hippocampal phosphorylated tau accumulation in various neurodegenerative disorders. *PLoS One.* 2011;6:e26996.
- Kurdi M, Chin E, Ang LC. Granulovacuolar degeneration in hippocampus of neurodegenerative diseases: quantitative Study. *J Neurodegener Dis.* 2016;2016:6163186.
- Castellani RJ, Gupta Y, Sheng B, et al. A novel origin for granulovacuolar degeneration in aging and Alzheimer's disease: parallels to stress granules. *Lab Invest.* 2011;91:1777-1786.
- Thal DR, Del Tredici K, Ludolph AC, et al. Stages of granulovacuolar degeneration: their relation to Alzheimer's disease and chronic stress response. *Acta Neuropathol.* 2011;122:577-589.
- Yamaguchi Y, Ayaki T, Li F, et al. Phosphorylated NF-kappaB subunit p65 aggregates in granulovacuolar degeneration and neurites in neurodegenerative diseases with tauopathy. *Neurosci Lett.* 2019;704:229-235.
- Truban D, Hou X, Caulfield TR, Fiesel FC, Springer W. PINK1, Parkin, and mitochondrial quality control: what can we learn about Parkinson's Disease Pathobiology?. *J Parkinsons Dis.* 2017;7:13-29.
- Fiesel FC, Ando M, Hudec R, et al. (Patho-)physiological relevance of PINK1-dependent ubiquitin phosphorylation. *EMBO Rep.* 2015;16:1114-1130.
- Fiesel FC, Springer W. Disease relevance of phosphorylated ubiquitin (p-S65-Ub). *Autophagy.* 2015;11:2125-2126.
- Hou X, Fiesel FC, Truban D, et al. Age- and disease-dependent increase of the mitophagy marker phospho-ubiquitin in normal aging and Lewy body disease. *Autophagy.* 2018;14:1404-1418.
- Fang EF, Hou Y, Palikaras K, et al. Mitophagy inhibits amyloid-beta and tau pathology and reverses cognitive deficits in models of Alzheimer's disease. *Nat Neurosci.* 2019;22:401-412.
- Cummins N, Tweedie A, Zuryn S, Bertran-Gonzalez J, Gotz J. Disease-associated tau impairs mitophagy by inhibiting Parkin translocation to mitochondria. *EMBO J.* 2019;38:e99360.
- Du F, Yu Q, Yan S, et al. PINK1 signalling rescues amyloid pathology and mitochondrial dysfunction in Alzheimer's disease. *Brain.* 2017;140:3233-3251.
- Ye X, Sun X, Starovoytov V, Cai Q. Parkin-mediated mitophagy in mutant hAPP neurons and Alzheimer's disease patient brains. *Hum Mol Genet.* 2015;24:2938-2951.
- Ramsden M, Kotilinek L, Forster C, et al. Age-dependent neurofibrillary tangle formation, neuron loss, and memory impairment in a mouse model of human tauopathy (P301L). *J Neurosci.* 2005;25:10637-10647.
- Borchelt DR, Thinakaran G, Eckman CB, et al. Familial Alzheimer's disease-linked presenilin 1 variants elevate Abeta1-42/1-40 ratio in vitro and in vivo. *Neuron.* 1996;17:1005-1013.
- Murray ME, Lowe VJ, Graff-Radford NR, et al. Clinicopathologic and 11C-Pittsburgh compound B implications of Thal amyloid phase across the Alzheimer's disease spectrum. *Brain.* 2015;138:1370-1381.
- Dickson DW, Crystal HA, Mattiace LA, et al. Identification of normal and pathological aging in prospectively studied nondemented elderly humans. *Neurobiol Aging.* 1992;13:179-189.
- Liu CC, Zhao N, Fu Y, et al. ApoE4 accelerates early seeding of amyloid pathology. *Neuron.* 2017;96:1024-1032.e3.
- Yue M, Hinkle KM, Davies P, et al. Progressive dopaminergic alterations and mitochondrial abnormalities in LRRK2 G2019S knock-in mice. *Neurobiol Dis.* 2015;78:172-195.
- Ghoshal N, Smiley JF, DeMaggio AJ, et al. A new molecular link between the fibrillar and granulovacuolar lesions of Alzheimer's disease. *Am J Pathol.* 1999;155:1163-1172.
- Fu H, Hardy J, Duff KE. Selective vulnerability in neurodegenerative diseases. *Nat Neurosci.* 2018;21:1350-1358.
- Kerr JS, Adriaanse BA, Greig NH, et al. Mitophagy and Alzheimer's disease: cellular and molecular mechanisms. *Trends Neurosci.* 2017;40:151-166.
- Corsetti V, Florenzano F, Atlante A, et al. NH2-truncated human tau induces deregulated mitophagy in neurons by aberrant recruitment of Parkin and UCHL-1: implications in Alzheimer's disease. *Hum Mol Genet.* 2015;24:3058-3081.
- Martin-Maestro P, Gargini R, Perry G, Avila J, Garcia-Escudero V. PARK2 enhancement is able to compensate mitophagy alterations found in sporadic Alzheimer's disease. *Hum Mol Genet.* 2016;25:792-806.
- Guerrero R, Navarro P, Gallego E, Garcia-Cabrero AM, Avila J, Sanchez MP. Hyperphosphorylated tau aggregates in the cortex and hippocampus of transgenic mice with mutant human FTDP-17 Tau and lacking the PARK2 gene. *Acta Neuropathol.* 2009;117:159-168.
- Rodriguez-Navarro JA, Gomez A, Rodal I, et al. Parkin deletion causes cerebral and systemic amyloidosis in human mutated

- tau over-expressing mice. *Hum Mol Genet.* 2008;17:3128-3143.
42. Hong X, Liu J, Zhu G, et al. Parkin overexpression ameliorates hippocampal long-term potentiation and beta-amyloid load in an Alzheimer's disease mouse model. *Hum Mol Genet.* 2014;23:1056-1072.
43. Reddy PH, Beal MF. Amyloid beta, mitochondrial dysfunction and synaptic damage: implications for cognitive decline in aging and Alzheimer's disease. *Trends Mol Med.* 2008;14:45-53.
44. Wiersma VI, van Ziel AM, Vazquez-Sanchez S, et al. Granulovacuolar degeneration bodies are neuron-selective lysosomal structures induced by intracellular tau pathology. *Acta Neuropathol.* 2019;138:943-970.
45. Okamoto K, Hirai S, Iizuka T, Yanagisawa T, Watanabe M. Reexamination of granulovacuolar degeneration. *Acta Neuropathol.* 1991;82:340-345.
46. Mrdjen D, Fox EJ, Bukhari SA, Montine KS, Bendall SC, Montine TJ. The basis of cellular and regional vulnerability in Alzheimer's disease. *Acta Neuropathol.* 2019;138:729-749.
47. Lee JH, Rao MV, Yang DS, et al. Transgenic expression of a ratiometric autophagy probe specifically in neurons enables the interrogation of brain autophagy in vivo. *Autophagy.* 2019;15:543-557.
48. McWilliams TG, Prescott AR, Allen GF, et al. mito-QC illuminates mitophagy and mitochondrial architecture in vivo. *J Cell Biol.* 2016;214:333-345.
49. Sun N, Yun J, Liu J, et al. Measuring in vivo mitophagy. *Mol Cell.* 2015;60:685-696.
50. Carosi JM, Sargeant TJ. Rapamycin and Alzheimer disease: a double-edged sword? *Autophagy.* 2019;15:1460-1462.
51. Watzlawik JO, Hou X, Truban, D, et al. Sensitive ELISA-based detection method for the mitophagy marker p-S65-Ub in human cells, autopsy brain, and blood samples. *Autophagy.* 2020. accepted.

#### SUPPORTING INFORMATION

Additional supporting information may be found online in the Supporting Information section at the end of the article.

**How to cite this article:** Hou X, Watzlawik JO, Cook C, et al. Mitophagy alterations in Alzheimer's disease are associated with granulovacuolar degeneration and early tau pathology. *Alzheimer's Dement.* 2021;17:417-430.  
<https://doi.org/10.1002/alz.12198>